

Article

Fabrication of ultralow stress TiO₂/SiO₂ optical coatings by plasma ion-assisted deposition

Chun Guo^{1,2,*}, Mingdong Kong¹

¹ Institute of Optics and Electronics, Chinese Academy of Sciences, Chengdu, China; guochun@ioe.ac.cn(C.G.); kongmd@ioe.ac.cn(M.K.);

² Key Laboratory of Optical Engineering, Chinese Academy of Sciences, Chengdu, China

* Correspondence: guochun@ioe.ac.cn

Abstract: Optical and mechanical properties of multilayer coatings depend on the selected layer materials and the deposition technology; therefore, knowledge of the performances of thin films is essential. In the present work, titanium dioxide (TiO₂) and silicon dioxide (SiO₂) thin films have been prepared by plasma ion-assisted deposition (PIAD). The optical, structural, and mechanical properties of thin films have been investigated using spectrometer/ellipsometer, X-ray diffraction (XRD), atomic force microscopy (AFM), and laser interferometer. The results show that TiO₂ film fabricated by PIAD induces a high refractive index, wide optical band gap, amorphous structure, smooth surface, and tensile stress. In the case of SiO₂ film, high bias voltage leads to dense structure and compressive stress. As an application, a three-wavelength high reflectance at 632.8, 808, and 1550nm is optimized and deposited. The dependence of total stress in the multilayer on the substrate temperature is studied as well. In conclusion, it is demonstrated that PIAD is an effective method for the preparation of ultralow stress TiO₂/SiO₂ multilayer films. The achieved stress is as low as 1.4MPa. The result could provide guidance to the stress optimization of most optical components without prefiguring, backside coating, and post-deposition treatments.

Keywords: stress; plasma ion-assisted deposition; TiO₂ film; SiO₂ film; annealing treatment.

1. Introduction

High-performance components for precision optics applications require thin films with perfect optical properties as well as minimal mechanical stress. As a result, it is crucial to select the coating materials and the deposition technology very carefully. In general, metal oxides (SiO₂, Al₂O₃, HfO₂, Ta₂O₅, Nb₂O₅, and TiO₂) and metal fluorides (MgF₂ and Na₃AlF₆) are common layer materials applied for [coating design in the visible and near-infrared spectral range](#). Conventional electron beam evaporation (EBE) remains the preferred vacuum coating technology for nanosecond pulsed laser devices[1,2]. Plasma-ion-assistance deposition (PIAD) and magnetron sputtering (MS) have been successfully employed for femtosecond laser systems[3,4]. Meanwhile, ion beam sputtering (IBS) has been comprehensively demonstrated for the preparation of high reflectivity and ultralow loss films in the advanced gravitational waves interferometers[5,6]. With the development of vacuum coating technology, the complexity of thin films has significantly increased, mechanical stress control has become a major challenge. Excessive stress can cause delamination, deformation, or cracks, severely affecting the properties and the stability of thin-film devices[7-10]. Therefore, the optimization of mechanical stress is very much necessary for the better performance of optical coatings.

The tensile or compressive stresses in thin films depend on many factors, such as deposition technique[11], substrate material[12], substrate temperature during preparation[9], layer material[7],

deposition rate[13], work gas pressure[14], etc. Up to now, several methods have been applied to manipulate the mechanical stress of thin films. Firstly, the substrate can be pretreated to an opposite surface figure either during the polishing process or before coating with a special nonuniform matching layer, so that prefiguring the coated surface can be offset the net effect of film stress[15,16]. In principle, these approaches need to determine the stress characteristics of optical coatings in advance, and preprocessing the optical surface is challenging for an optical element with complex geometry. Secondly, layer materials with opposite stress can be employed to decrease the multilayer stress, although the available materials are very limited[7,11]. Thirdly, backside coatings and thermal annealing treatment have been commonly used to control stress-induced deformation, the corresponding operation and disadvantage of the approaches are reviewed in other literature[4,11,13,17-20]. Besides, thermal oxide patterning and ion implantation have successfully used to compensate film stress in thin silicon substrates for X-ray optical applications[21,22]. Nevertheless, the methods have limitations as well. Last but not least, since thin films fabricated by EBE and PIAD can be manipulated as tensile or compressive stress[7,23,24], while the films prepared using MS and IBS are commonly compressive stress[9,11,17]. It is possible to realize stress control by combining several coating technologies. Tajima et al.[23] have studied the stress control of SiO₂ film by simultaneous sputtering and EBE. As a result, the obtained stress of SiO₂ film prepared with the proposed method is approximately 60% of that by EBE and one-fourth of that by sputtering. Woo et al.[24] have reported the stress optimization for a TiO₂/MgF₂ narrow band-pass filter. The destructive tensile stress in the EBE MgF₂ films can be counteracted by the compressive stress of the PIAD TiO₂ films, consequently without microcracks in the multilayer. Liu et al.[25] have investigated the stress compensation for anti-reflection coating, which is designed and fabricated with IBS SiO₂ and atomic layer deposition Al₂O₃. Finally, the stress is as low as 38MPa. Taken the efficiency and cost of stress control technology as well as the optical and environmental stability of optical coatings into consideration, PIAD is still the best choice for the preparation of ultralow stress films.

In the present work, titanium dioxide (TiO₂) and silicon dioxide (SiO₂) have been chosen for the optical coatings due to the high refractive index contrast, which can simplify the optical design, then reduce the residual stress. Single layers of TiO₂ and SiO₂ as well as a three-wavelength high reflection (HR) are prepared by PIAD. Detailed results for the optical, mechanical, and environmental properties are characterized and discussed. It suggests that thin films having perfect optical performance and ultralow stress can be realized with the optimization of the deposition parameters.

2. Materials and Methods

TiO₂ and SiO₂ films were prepared by a Leybold SYRUS pro 1110 DUV vacuum system, consisting of an advanced plasma source (APS), two electron beam guns, and four ceramic heaters. The APS was used to bombard a growing film with argon (Ar) and oxygen (O₂) ions. In the coating process, a base pressure approximately 2.0×10^{-4} Pa was ensured in the vacuum chamber by a cryopump set. Fused silica plates and silicon wafers with a root-mean-square surface roughness of approximately 0.5nm were used as the substrates. The distance between the evaporation source and the substrate was approximately 750mm. Before the deposition, substrates were first treated manually with alcohol and acetone in a standard laboratory environment. Then, they were cleaned with Ar plasma formed by the APS in the vacuum chamber to remove potential contaminations. High-purity Ti₂O₃ and SiO₂ grains (Merck) were used as starting materials. The physical thickness and deposition rate of thin films were controlled by a quartz-crystal monitor, which was positioned at the top center of the deposition chamber. TiO₂ and SiO₂ were fabricated by the PIAD at a substrate temperature of 180 °C. The deposition rates of TiO₂ and SiO₂ films were set to 0.2 and 0.4nm/s, respectively, and the thickness of the TiO₂ and SiO₂ films was kept at about 350nm and 900nm. High purity O₂ (99.999%) was employed to improve the stoichiometric ratio of the thin films. The plasma source is set to constant bias voltage and discharge current mode. Further details for the deposited TiO₂ and SiO₂ films were summarized in Table 1. After the deposition processes were finished, the samples were allowed to cool down to room temperature, and the vacuum chamber was vented.

Table 1 Deposition parameters of TiO₂ and SiO₂ thin films

Material	Substrate temperature (°C)	Deposition rate (nm/s)	Bias voltage (V)	Discharge current (A)	Gas flow rate (sccm)	
					Ar	O ₂
TiO ₂	180	0.2	120	50	12	25
SiO ₂		0.4	140		12	5

The TiO₂ film on fused silica substrate was applied for the transmittance, thickness, optical constants, and energy band gap analysis. A Perkin Elmer Lambda 1050 spectrophotometer was used to measure the transmittance of TiO₂ film at a normal incident angle. SiO₂ film on silicon substrate was employed for thickness and refractive index determination with a variable-angle spectroscopic ellipsometer (VASE). The ellipsometric data were characterized at angles of incidence 65°, 70°, and 75°. The samples deposited on fused silica substrates were also used to analyze the microstructure, surface morphology, and stress of the TiO₂ and SiO₂ films. Microstructures of thin films were investigated with a Philips X'Pert-MRD XRD operated with Cu-K α radiation ($\lambda = 0.154$ nm) in symmetrical Φ -2 Φ geometry. The incident angle ranged from 10° to 80° with a step of 0.01°. The surface morphology was examined through a Veeco Dimension 3100 AFM, performing in a tapping mode for imaging surface with 5×5 μm and 256×256 sample points. A Zygo laser interferometer was used to evaluate the stress of TiO₂ and SiO₂ films by measuring the variation in curvatures of the substrate before and after deposition. The measurements were performed at the He-Ne laser wavelength ($\lambda=632.8\text{nm}$). The measurement accuracy of the optical interferometer was better than $\lambda/100$ for the surface flatness.

3. Results and Discussion

3.1. Single-layer coatings

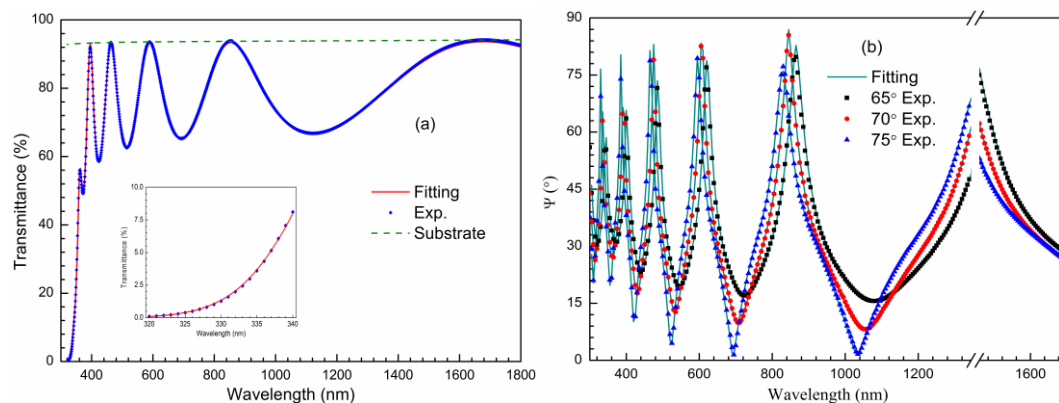


Figure 1. (a) Experimental transmittance spectra measured at normal incidence and best-fit curve for TiO₂ layer; (b) Experimental ellipsometric data (Ψ) measured at angles of incidence 65°(squares), 70°(circles), and 75°(triangles) and best-fit curves for the SiO₂ layer.

To fabricate multilayer coatings with optimizing optical and mechanical properties, it is necessary to investigate the performances of the deposited TiO₂ and SiO₂ single layers. The physical thickness and optical constants (n , k) of the TiO₂ film are determined from a spectrophotometric measurement. Transmittance spectra of the TiO₂ film and fused silica substrate in the range of 300-1800 nm with a 1 nm wavelength step are obtained by the PE Lambda 1050 spectrophotometer as presented in Figure 1 (a). The transmittance spectrum of TiO₂ film is lower than that of the substrate, meaning that the refractive index of TiO₂ film is higher than that of the substrate. The transmittance maxima of TiO₂ film are consistent with that of the substrate above 400nm. It indicates that the TiO₂ film is a negligible absorption and refractive index homogeneous layer in the visible

and near-infrared range. At shorter wavelengths, the spectrum deviation between TiO₂ film and substrate is caused by the absorption of TiO₂ film. In addition, fused silica is a transparent substrate in the interesting wavelength range. It has been well polished and has sufficient thickness to avoid surface interference on the spectral measurement. The transmission of a single layer absorbing film is a function of the refractive index (n), extinction coefficient (k), physical thickness (d), and the wavelength of light (λ). In our characterization process, the functional forms of $n(\lambda)$ and $k(\lambda)$ are described by Tauc-Lorentz model[26]. The imaginary part (ε_2) of the complex dielectric function $\varepsilon = \varepsilon_1 - i\varepsilon_2 = (n - ik)^2$ is defined by

$$\varepsilon_2(E) = \begin{cases} \frac{AE_0\Gamma(E-E_g)^2}{(E^2-E_0^2)^2 + \Gamma^2E^2} \frac{1}{E}, & E > E_g \\ 0, & E \leq E_g \end{cases} \quad (1)$$

Where A , E_0 , E_g and Γ denote amplitude, peak transition energy, band gap energy, and broadening parameter, respectively. $E = hc/\lambda$ is photon energy, h and c represent the Planck's constant and the velocity of light in vacuum. The real part (ε_1) of the dielectric function is achieved using analytical integration of the Kramers-Körnig relation:

$$\varepsilon_1(E) = \varepsilon_\infty + \frac{2}{\pi} (C.P.) \int_0^\infty \frac{\xi \varepsilon_2(\xi)}{\xi^2 - E^2} d\xi \quad (2)$$

Where ($C.P.$) denotes the Cauchy principal value of the integral. ε_∞ represents the contribution of the optical transition at higher energies. The constants d , A , E_0 , Γ , E_g and ε_∞ are fitting parameters. The fitting is then performed by minimizing the squared difference between the experimentally measured and calculated transmittance values. The optimal selection approach of these parameters is carried out using the particle swarm optimization algorithm[27]. After a fine adjustment of the settings, a proper fitting can be obtained, and then the optical constants and thickness of thin film are determined.

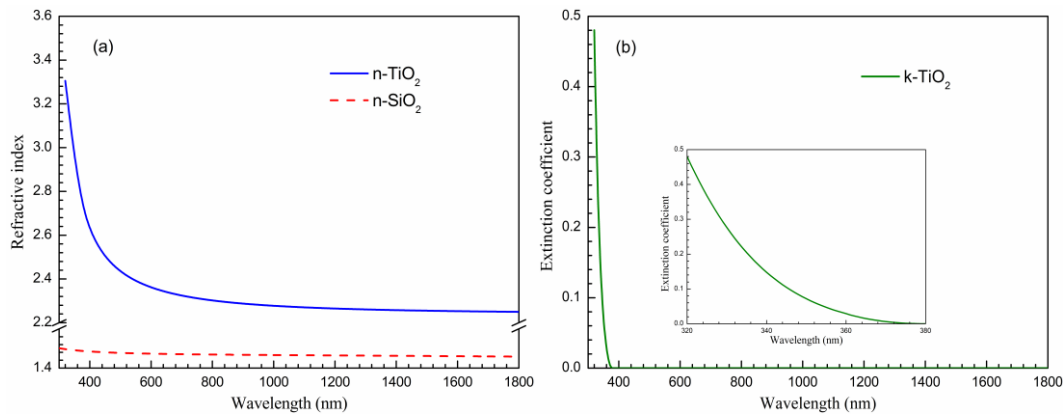


Figure 2. (a) Refractive index of TiO₂ (solid curve) and SiO₂ (dashed line) films; (b) extinction coefficient of TiO₂ film.

The experimental and calculated transmittances are in good agreement, as exhibited in Figure 1(a). The average discrepancies at wavelengths shorter than 400nm are ~0.45%, ~0.15% in the entire wavelength range. It is demonstrated that the Tauc-Lorentz model gives good results in the determination of optical constants of the TiO₂ film near the cut-off wavelength. The best-fitting thickness of the TiO₂ film is 372.9nm, listed in Table 2. The values of the parameters in the Tauc-Lorentz expressions Eqs. (1) and (2) are $A=193.29$ eV, $E_0=4.47$ eV, $\Gamma=1.60$ eV, $E_g=3.24$ eV and $\varepsilon_\infty=1.86$. The obtained wavelength dependence of the refractive index is shown in Figure 2(a) by the solid curve. The refractive index at 500nm is 2.436. As expected, the refractive index of the

TiO₂ film deposited by PIAD is larger than that of EBE (2.358) and smaller than that of IBS (2.508) [28,29]. It is not surprising that the higher the deposition energy, the denser the film structure, and the greater the refractive index.

Table 2 Thickness, refractive index at 500nm, energy band gap, surface roughness, phase composition and stress of TiO₂ and SiO₂ thin films

Material	Thickness (nm)	Refractive index	Energy band gap (eV)	RMS Roughness (nm)	Phase composition	Stress (MPa)
TiO ₂	372.9	2.436	3.34-3.38	0.52	amorphous	+164.8
SiO ₂	936.7	1.477	/	1.39		-395.8

Moreover, the optical band gap of the TiO₂ film is calculated with the help of Tauc plots. For indirect band gap, the absorption coefficient α is a function of the photon energy E in the following equation[30]:

$$\alpha(E) = \frac{B(E - E_g)^2}{E} \quad (3)$$

where B is a fitting constant. From Eq. (3), it can be seen that $(\alpha E)^{1/2}$ has a linear dependence on E . Thus, by plotting $(\alpha E)^{1/2}$ versus E , the optical band gap E_g can be determined from extrapolating the linear fit to zero. The absorption coefficient is calculated through extinction coefficient $k(\lambda)$:

$$\alpha = \frac{4\pi}{\lambda} k(\lambda) \quad (4)$$

the extinction coefficient $k(\lambda)$ is obtained from spectrophotometric measurement. On the other hand, in a high-absorption spectral range, the absorption coefficient α is related to the transmittance T and physical thickness d of thin-film based on Beer's law[29]:

$$\alpha \approx \frac{1}{d} \ln\left(\frac{1}{T}\right) \quad (5)$$

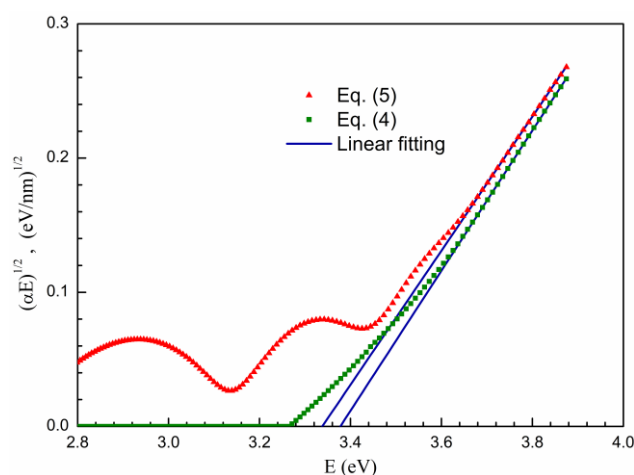


Figure 3. The variation of the square of the absorption coefficient $(\alpha E)^{1/2}$ versus the photon energy E of TiO₂ thin film, triangle and square data calculated from Eq. (4) and (5), solid lines: corresponding linear fits.

In order to reduce the influence of spectral measurement error on the accuracy of the calculated coefficients, the transmittance spectrum near the cutoff edge (above 0.1%) is applied to the

determinations of the absorption coefficient and extinction coefficient. In Figure 3, the Tauc plots for the indirect band gap and the corresponding linear fits for the TiO₂ film deposited by PIAD are presented. The optical band gaps linear fitted using Eqs. (4) and (5) are 3.38 and 3.34 eV, respectively. They are quite close to each other, which is due to the successful application of the Tauc-Lorentz model for the parameterization of the optical constants of thin-film near the absorption edge. As shown in the illustration in Figure 1 (a), the deviation between the experimental and calculated transmittances is less than 0.1% in the wavelength range from 320 to 340nm. The result can be considered as the accuracy of optical band gap determination in this investigation. In general, the optical band energies obtained by Eqs. (4) and (5) are commonly larger than that determination from the Tauc-Lorentz model.

For the SiO₂ film, it is difficult to directly investigate a single layer deposited on the fused silica substrate since there is no refractive index contrast and no variation in transmittance with respect to the wavelength. To overcome the problem, a considerable difference in transmission can be achieved with a double-layer structure consisting of a thin TiO₂ layer and thick SiO₂. As expected, the thickness and refractive index of SiO₂ film can be estimated by fitting the transmission curve with commercial software like OptiRE [31]. The method has been introduced in detail in the previous research paper[32]. Besides, ellipsometric measurement is an excellent choice to determine the parameters of the SiO₂ film deposited on Si substrate[33]. In this case, the reflection ellipsometry data are characterized in the range of 300-1700 nm using the VASE. The data analysis is performed with a reasonable assumption. The SiO₂ film is treated to be non-absorbing, as the extinction coefficient is lower than 1.0×10^{-4} in the interesting wavelength range and has a negligible impact on the ellipsometry data. The ellipsometric parameters Ψ and Δ are simultaneously fitted with thickness and refractive index. Wavelength dependency of SiO₂ refractive index is described by Sellmeier:

$$n^2 = 1 + \frac{A_1(\lambda/\lambda_0)^2}{(\lambda/\lambda_0)^2 - A_2} + \frac{A_3(\lambda/\lambda_0)^2}{(\lambda/\lambda_0)^2 - A_4} + \frac{A_5(\lambda/\lambda_0)^2}{(\lambda/\lambda_0)^2 - A_6} \quad (6)$$

where A_1, \dots, A_6 are dimensionless parameters, $\lambda_0 = 1000\text{nm}$, the unit of λ is nanometer. Figure 1 (b) shows the experimental Ψ data and the best-fit curves of the SiO₂ single layer at angles of incidence 65°, 70°, and 75°. It can be seen that the measured data are well fitted with the method. The thickness of the SiO₂ film is characterized by 936.7 nm. The determining refractive index of SiO₂ film is presented in Figure 2a with the dashed line. The parameters in the Sellmeier expressions are $A_1 = 4.842825$, $A_2 = 1.332323$, $A_3 = 6.650996$, $A_4 = 2.796139$, $A_5 = 100.0728$, and $A_6 = 1275.594$. For the SiO₂ film deposited by PIAD at the 140V bias voltage, the refractive index at 500nm, which is larger than that of fused silica substrate (1.4623), is equal to 1.477.

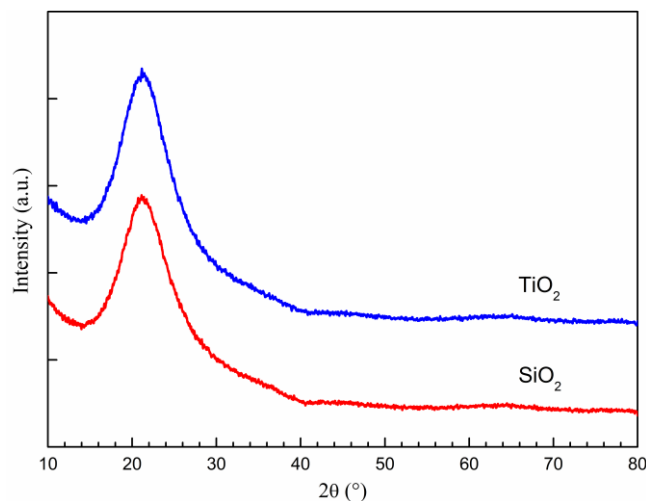


Figure 4. XRD patterns of TiO₂ and SiO₂ thin films deposited by PIAD.

Figure 4 presents the XRD patterns of thin films deposited on fused silica substrates. The absence of any sharp diffraction peaks and the presence of hump indicate the amorphous phase of the TiO₂ and SiO₂ films prepared by PIAD technology at the substrate temperature of 180°C. The surface morphologies of thin films are investigated by AFM over 5 × 5 μm² areas. Figure 5 shows typical morphologies of the TiO₂ and SiO₂ films. The RMS roughness of the surface is calculated by the definition[30]:

$$RMS = \sqrt{\frac{\sum_{i=1}^N (z_i - z_{avg})^2}{N-1}} \quad (7)$$

where z_i is the current value of z , z_{avg} is the average value of z on the scanned area, N is the number of points in the image. Experimentally, the RMS roughness of TiO₂ and SiO₂ films are determined to 0.52nm and 1.39nm, respectively. It is exhibited that the surface roughness of TiO₂ film is smaller than that of SiO₂ film attributed to the larger physical thickness of the latter.

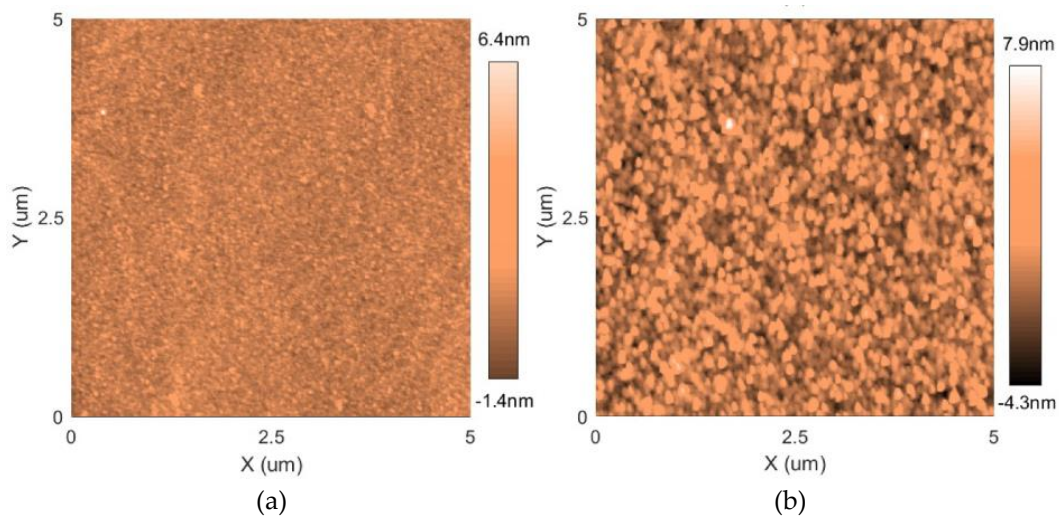


Figure 5. AFM topography images of TiO₂ (a) and SiO₂ (b) thin films.

Stress measurements of the TiO₂ and SiO₂ single layers are carried out with a Zygo laser interferometer by characterizing the reflected wavefront deformation of fused silica substrates. The stress of thin film is calculated by the Stoney equation[34]:

$$\sigma = \frac{E_s t_s^2}{6(1-\nu_s) d_f} \left(\frac{1}{R_1} - \frac{1}{R_0} \right) \quad (8)$$

$$R \approx \frac{D^2}{8P} \quad (9)$$

where, E_s and ν_s are Young's modulus and Poisson's ratio of the substrate, t_s and d_f are the thicknesses of the substrate and deposited thin film, R_0 and R_1 are the radii of curvatures of the substrate before and after deposition. P is the power of reflected wavefront mapping, D is the diameter of the clear aperture. In the present work, the nominal thickness and diameter of fused silica substrates are 3 and 40 mm. E_s and ν_s of fused silica are 72 GPa and 0.17. For the preparation of TiO₂ and SiO₂ films, the measured variations of reflected wavefront mapping are determined and presented in Figure 6. It can be seen that after the deposition of 372.9nm TiO₂ and 936.7nm SiO₂ films, the power values of the reflected wavefront of these substrates are changed with 0.151 and -0.911 λ ($\lambda=632.8$ nm). Accordingly, the calculated stresses of the TiO₂ and SiO₂ films from Eqs. (8) and (9) are +164.8 and -395.8 MPa. Here positive and negative stress values represent tensile and compressive stress, respectively. As demonstrated in [7,20,35], when the thin film is taken out of the deposition chamber, the adsorption of water can lead to a strong evolution of the stress over

time. Thereby, it is important to keep in mind that thin film should be stored in a normal laboratory environment for a long time. Then the surface figure is measured to obtain the final stable stress behavior. The stress data presented in work are measured after at least four weeks of storage if there is no other statement.

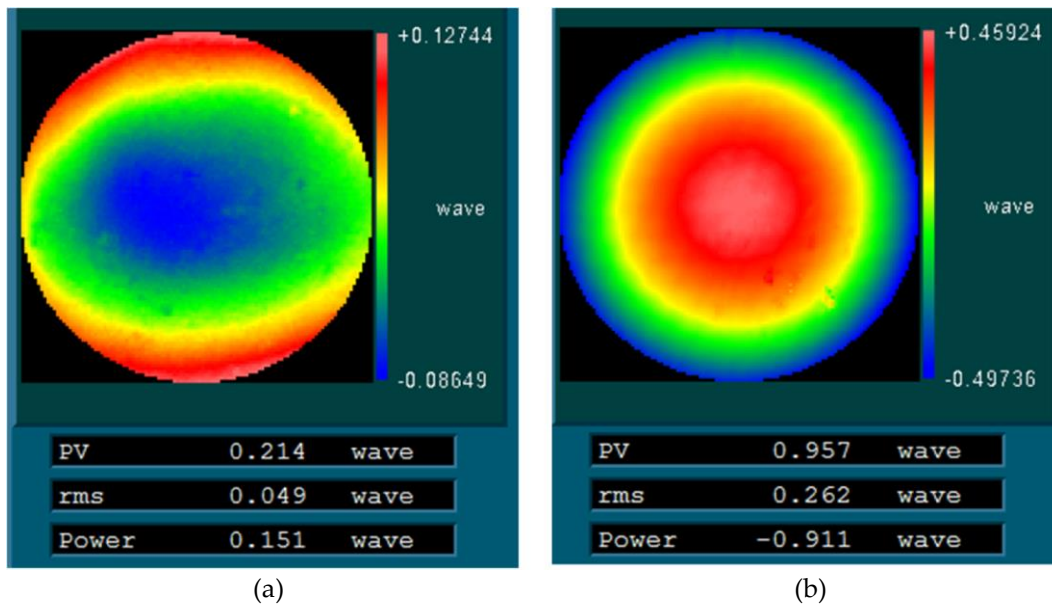


Figure 6. Surface figures of TiO₂ (a) and SiO₂ (b) thin films fabricated by PIAD.

3.2. Multilayer coatings

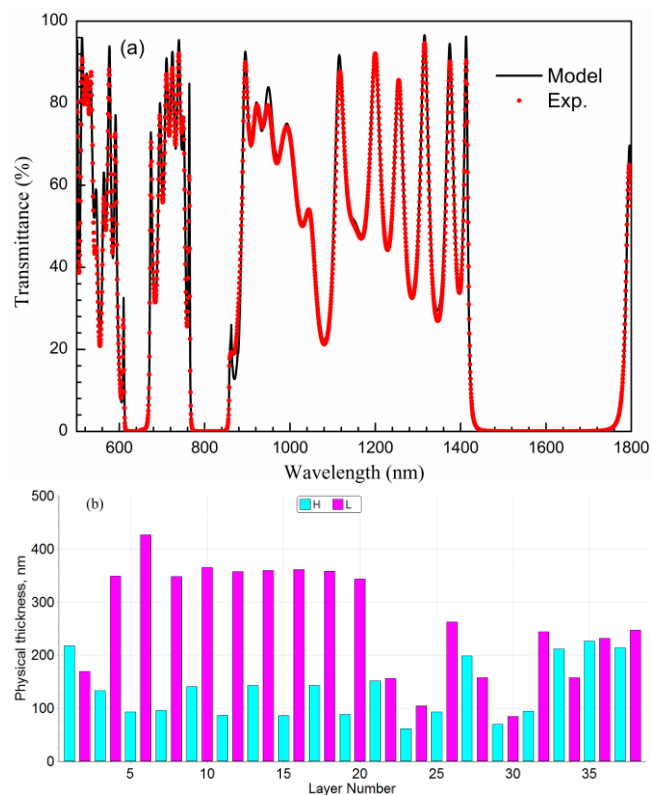


Figure 7. (a) Transmittance spectra of experimental (circles) and theoretical design (solid curve) for the TiO₂/SiO₂ multilayer; (b) Layer thickness profile of optical coating.

Based on the results of TiO₂ and SiO₂ films, a three-wavelength HR is optimized and fabricated on the fused silica substrate. For the multilayer coating design, the performance target is reflectivity

greater than 99.95% at wavelengths of 632.8, 810, and 1550 nm. Taking into consideration the feasibility and repeatability, each working wavelength has a band with width of at least 30nm. To obtain better environmental durability, the outermost layer of optical coatings is SiO₂ with a thickness of at least 200 nm. The structure of the three-wavelength HR is optimized with the help of a needle technique incorporated into the OptiLayer software[31]. The theoretical transmission spectrum and layer thickness profile of the final 38-layer coating design are exhibited in Figure 7. The total thicknesses are 3020.51 nm for TiO₂ material and 3802.26 nm for SiO₂ material, leading to a total coating thickness of 6822.77 nm. The calculated reflectance is higher than 99.99% in the interesting wavelengths. The preparation of such a design with a 38-layer structure of nonquarter-wave optical thickness is a challenging task. In our experiment, the deposition parameters for multilayer coating are the same as those for the TiO₂ and SiO₂ single layers in Table 1. The layer thicknesses of the multilayer coating are controlled with the quartz crystal monitor. To obtain ideal optical properties, the thickness errors of thin films are corrected with the help of OptiRE software.

After the deposition, the optical performance of fabricated three-wavelength HR is characterized by the Perkin Elmer Lambda 1050 spectrophotometer in the range from 500 to 1800 nm. The measured and calculated transmittance curves are presented in Figure 7a. Good agreement between the theory and experiment is achieved. The residual transmittance values at wavelengths of 632.8, 810, and 1550 nm are smaller than 0.01%. The reflected wavefront performance is measured with the Zygo laser interferometer. Figure 8c shows the coating deformation for the fused silica along with the difference between the pre-coating and the as-deposited surface measurement. The optical power variation of -0.026 wave at 632.8 nm corresponds to a compressive stress of 1.4 MPa based on Eqs. (8) and (9). It is proved that the fabrication of ultralow stress optical coatings can be realized by optimizing the combination of film materials and the deposition technique.

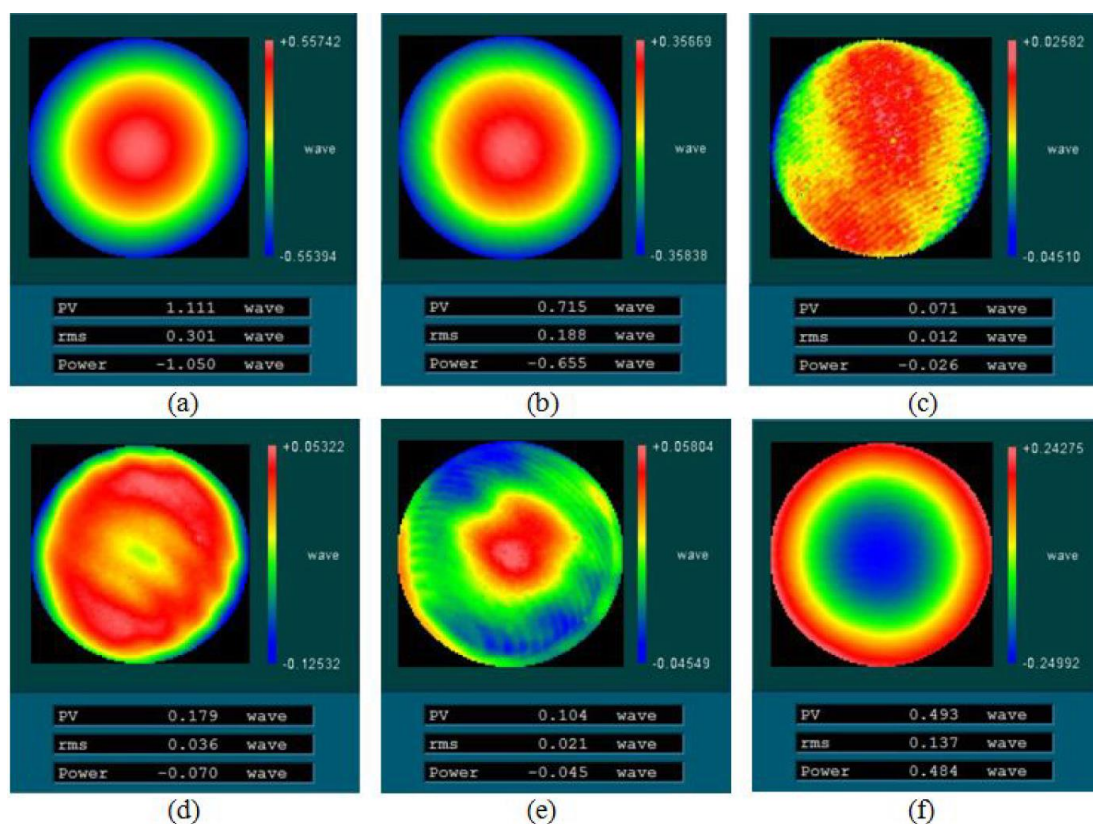


Figure 8. Surface figures of TiO₂/SiO₂ multilayer prepared at different deposition temperatures. As deposited: (a) 120°C; (b) 150°C; (c) 180°C; (f) 210°C; Annealing treatment: (d) 120°C and (e) 150°C.

On the other hand, the total stress of the multilayer coating is a function of the film thickness and stress of each constituent material in the design and given by the following formula[7,24]:

$$\sigma_{total} = \frac{\sum_{i=1}^m \sigma_i d_i}{\sum_{i=1}^m d_i} \quad (10)$$

where σ_i and d_i are the stress and thickness of the i layer, m is the maximum number of layers in optical coatings design. Based on the previously measured stresses of the TiO₂ and SiO₂ single layers and the thicknesses of each layer in the design, the calculated total stress of the 38-layer design is compressive stress of -147.7 MPa. The reason for the deviation between the theoretical calculation and the experimental result is that the multilayer deposition time is longer than that of single layers at the same substrate temperature. Since the stress of thin-film depends on the deposited materials' microstructure, the evolution of the film microstructure during deposition is related to the substrate temperature. In particular, the high substrate temperature is prevalent for reducing compressive stress, just like annealing treatment.

Table 3 Total stress of TiO₂/SiO₂ multilayer as-deposited and annealing treatment

Deposition temperature (°C)	Stress (MPa)	
	As-deposited	Annealing treatment
120	-56.4	-3.8
150	-35.2	-2.4
180	-1.4	/
210	+25.9	/

For a further understanding of the substrate temperature dependency of the total stress of the 38-layer design, different substrate temperatures are used for the fabrication of the multilayer coatings. Experimentally, three different substrate temperatures of 120, 150, and 210 °C are chosen. Reflected wavefront deformations of the fused silica substrates as deposition are exhibited in Figures 8a, 8b, and 8f, respectively. The optical power variations are -1.050, -0.655, and 0.484 waves. Meanwhile, the total stresses of the multilayer coatings are -56.4, -35.2, and 26.0 MPa, as shown in Figure 9 and Table 3. It is notable, from these results, that the final film stress of the 38-layer design is near zero at a specific substrate temperature, the tensile stress of TiO₂ completely compensates the compressive stress of SiO₂.

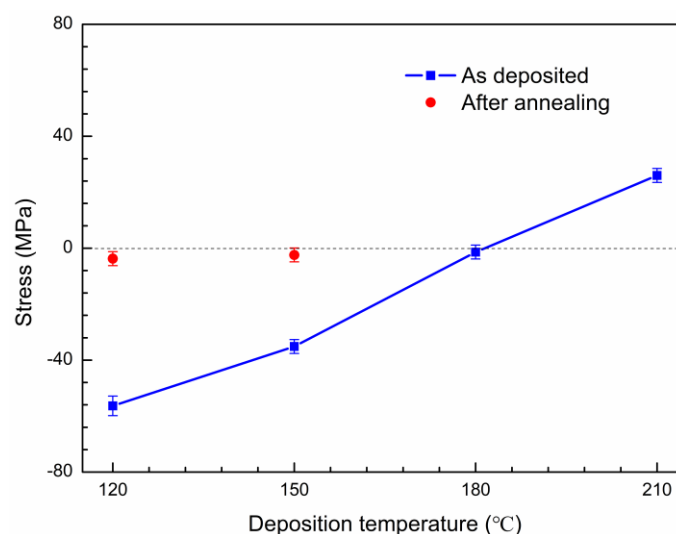


Figure 9. The stress of TiO₂/SiO₂ multilayer deposited at various temperatures before and after annealing treatment.

Experimentally, multilayer coating deposited at the substrate temperatures below 180°C is compressive stress. As it is well known that the postdeposition annealing treatment is a good choice for reducing compressive stress in optical coatings[11,18]. In the case, thermal annealing in air is performed in a heating furnace ensuring temperature repeatability of less than 2°C. Thin films having compressive stress are annealed in the air to 180°C temperature. The annealing routine consists of three parts: heating phase, constant annealing phase, and cooling phase. At heating phase temperature is linearly increased by 2°C per minute until the target annealing temperature is reached. During constant annealing phase temperature remains stable for four hours. At the cooling phase temperature is dropped by 2°C per minute until room temperature is reached. After annealing treatment, reflected wavefront mappings of the TiO₂/SiO₂ multilayer coatings on fused silica substrates are characterized and presented in Figures 8d and 8e. The postdeposition annealing total stresses of multilayer coatings deposited at substrate temperatures of 120 and 150°C are optimized to be -3.8 and -2.4 MPa, respectively. Obviously, the total stresses of low-temperature deposition films after annealing treatments are approximately equivalent to that of multilayer coating prepared by the best substrate temperature. For tensile stress film, such as three-wavelength HR coating fabricated at the substrate temperature of 210°C, there are few investigations on reducing stress by post-deposition treatment. The relatively feasible methods include processing the substrate into the opposite surface figure before coating or adding a particular matching layer into optical coatings design[15,16]. These strategies are not performed in the present research.

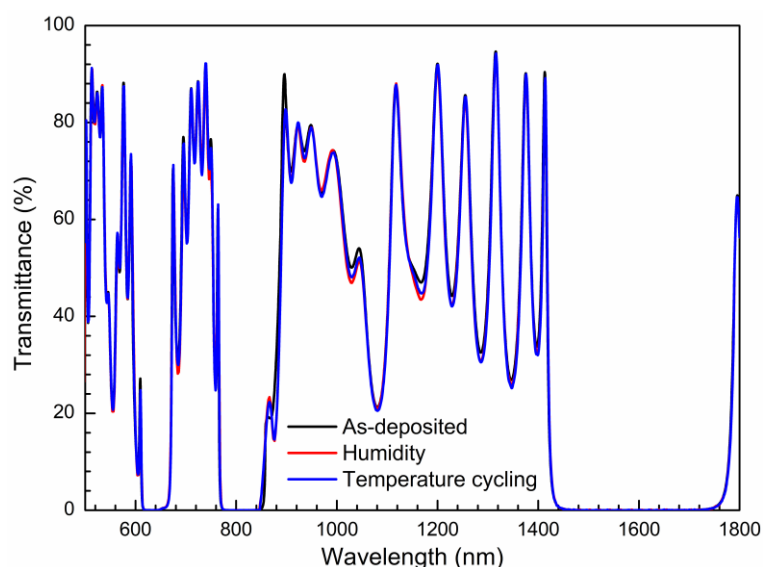


Figure 10. Transmittance spectra of as-deposited three-wavelength HR coatings, and after humidity and temperature cycling tests.

Environmental durability of the prepared three-wavelength HR coating is tested on the basis of temperature cycling and humidity requirements of the Chinese military specifications GJB150.5A-2009 and GJB150.9A-2009. Parameters for temperature cycling and humidity tests are consistent with Reference[32]. No physical damages are observed after temperature cycling and humidity tests, and no coatings are removed under adhesion test. Transmittance spectra of the prepared three-wavelength HR coating after both tests are also presented in Figure 10. There is no observable difference among these spectra. These results demonstrate that the PIAD deposited optical coatings have excellent environmental durability in terms of high/low temperature cycling and high humidity.

4. Conclusions

The reliable characterizations of TiO₂ and SiO₂ thin films fabricated by PIAD provide a basis for careful investigations of optical and mechanical stress properties of multilayer coatings using both layer materials. Single-layer TiO₂ and SiO₂ thin films were fabricated by PIAD on fused silica and

silicon substrates. Spectrophotometer/ellipsometer, XRD, AFM, and laser interferometer were adopted to investigate the optical and microstructural properties, such as optical constants, optical band gap, crystal structure, surface roughness, and reflected wavefront. Moreover, a three-wavelength HR consisting of TiO₂ and SiO₂ films is optimized and deposited. The dependence of total stress in the multilayer on the substrate temperature is studied in detail. These results would be of great importance to the preparation of ultralow stress optical coatings in the visible and near-infrared spectral range. These can be employed to most optical elements without prefiguring, backside coating, and post-deposition treatments.

Author Contributions: Conceptualization, C.G.; methodology, C.G.; validation, M.K.; formal analysis, C.G.; data curation, M.K.; writing—original draft preparation, C.G.; writing—review and editing, C.G..

Funding: This research was funded by the Youth Innovation Promotion Association of the Chinese Academy of Sciences and Sichuan Science and Technology Program.

Acknowledgments: We sincerely thank Weidong Gao, Junqi Fan, and Hui Wang of Institute of Optics and Electronics, Chinese Academy of Science for their generous assistance in XRD, AFM, and wavefront measurements, respectively.

Conflicts of Interest: The authors declare no conflict of interest.

References

1. Negres, R.A.; Stolz, C.J.; Thomas, M.D.; Caputo, M. 1064nm, nanosecond laser mirror thin film damage competition. *SPIE* **2018**, *10805*, 108050Y.
2. Stolz, C.J.; Negres, R.A.; Feigenbaum, E. Trends observed in 10 years of thin film coating laser damage competitions. in *Optical Interference Coatings Conference (OIC) 2019, OSA Technical Digest (Optical Society of America, 2019)* **2019**, paper ThA.1.
3. Oliver, J.B.; Bromage, J.; Smith, C.; Sadowski, D.; Dorrer, C.; Rigatti, A.L. Plasma-ion-assisted coatings for 15 femtosecond laser systems. *Appl. Opt.* **2014**, *53*, A221-A228.
4. Amotchkina, T.; Trubetskov, M.K.; Pervak, Y.; Veisz, L.; Pervak, V. Stress compensation with antireflection coatings for ultrafast laser applications: from theory to practice. *Opt. Exp.* **2014**, *22*, 30387-30393.
5. Pinard, L.; Sassolas, B.; Flaminio, R.; Forest, D.; Lacoudre, A.; Michel, C.; Montorio, J.L.; Morgado, N. Toward a new generation of low-loss mirrors for the advanced gravitational waves interferometers. *Opt. Lett.* **2011**, *36*, 1407-1409.
6. Degallaix, J.; Michel, C.; Sassolas, B.; Allocca, A.; Cagnoli, G.; Balzarini, L.; Dolique, V.; Flaminio, R.; Forest, D.; Granata, M., et al. Large and extremely low loss: the unique challenges of gravitational wave mirrors. *J. Opt. Soc. Am. A* **2019**, *36*, C85-C94.
7. Oliver, J.B.; Kupinski, P.; Rigatti, A.L.; Schmid, A.W.; Lambropoulos, J.C.; Papernov, S.; Kozlov, A.; Smith, C.; Hand, R.D. Stress compensation in hafnia/silica optical coatings by inclusion of alumina layers. *Opt. Exp.* **2012**, *20*, 16596-16610.
8. Oliver, J.B.; Smith, C.; Spaulding, J.; Rigatti, A.L.; Charles, B.; Papernov, S.; Taylor, B.; Foster, J.; Carr, C.W.; Luthi, R., et al. Glancing-angle-deposited magnesium oxide films for high-fluence applications. *Opt. Mater. Express* **2016**, *6*, 2291-2303.
9. Steinecke, M.; Kiedrowski, K.; Jupé, M.; Ristau, D. Very thick mixture oxide ion beam sputtering films for investigation of nonlinear material properties. *Eur. Phys. J. Appl. Phys.* **2017**, *80*, 30301-30305.
10. Zhang, Y.P.; Long, G.Y.; Zhou, H.; Fan, J.Q.; Cui, H.; Cheng, L. Finite-element-method study of the effect of thin-film residual stresses on high-order aberrations of deformable mirrors. *Surf. Coat. Technol.* **2019**, *366*, 35-40.

11. Kičas, S.; Gimževskis, U.; Melnikas, S. Post deposition annealing of IBS mixture coatings for compensation of film induced stress. *Opt. Mater. Express* **2016**, *6*, 2236-2243.
12. Tian, X.X.; Xiong, S.M.; Zhang, Y.H.; Zhang, K.P. Simulation of thermal stress in ion beam sputtered Ta₂O₅/SiO₂ multilayer coatings on different substrates by finite element analysis. *Surf Coat. Technol.* **2019**, *362*, 225-233.
13. Brossmann, J.; Lappschies, M.; Jakobs, S. Precisely stress compensated dielectric laser mirrors deposited by PARMS on thin deformable substrates. in *Optical Interference Coatings Conference (OIC) 2019, OSA Technical Digest (Optical Society of America, 2019)* **2019**, paper WC.6.
14. Biscwas, D.; Sinha, A.K.; Chakraborty, S. Effects of oxygen partial pressure and annealing temperature on the residual stress of hafnium oxide thin-films on silicon using synchrotron-based grazing incidence X-ray diffraction. *Appl. Surf. Sci.* **2016**, *384*, 376-379.
15. Oliver, J.B.; Spaulding, J.; Charles, B. Stress compensation by deposition of a nonuniform corrective coating. *App. Opt.* **2020**, *59*, A54-A57.
16. Gensemer, S.; Gross, M. Figuring large optics at the sub-nanometer level: compensation for coatings and gravity distortions. *Opt. Exp.* **2015**, *23*, 31171-31180.
17. Begou, T.; Lumeau, J. Accurate analysis of mechanical stress in dielectric multilayers. *Opt. Lett.* **2017**, *42*, 3217-3220.
18. Bischoff, M.; Nowitzki, T.; Voß, O.; Wilbrandt, S.; Stenzel, O. Postdeposition treatment of IBS coatings for UV applications with optimized thin-film stress properties. *Appl. Opt.* **2014**, *53*, A212-A220.
19. Lemarquais, F. Athermal compensation of the stress-induced surface deflection of optical coatings using iso-admittance layers. *Appl. Opt.* **2014**, *53*, A229-A236.
20. Denus-Baillargeon, M.; Schmitt, T.; Larouche, S.; Martinu, L. Design and fabrication of stress-compensated optical coatings: Fabry-Perot filters for astronomical applications. *Appl. Opt.* **2014**, *53*, 2616-2624.
21. Yao, Y.W.; Chalifoux, B.D.; Heilmann, R.K.; Schattenburg, M.L. Thermal oxide patterning method for compensating coating stress in silicon substrates. *Opt. Express* **2019**, *27*, 1010-1025.
22. Chalifoux, B.D.; Yao, Y.W.; Woller, K.B.; Heilmann, R.K.; Schattenburg, M.L. Compensating film stress in thin silicon substrates using ion implantation. *Opt. Express* **2019**, *27*, 11182-11195.
23. Tajima, N.; Murotani, H.; Matumoto, S.; Honda, H. Stress control of an optical thin film by sputtering and vacuum deposition. in *Optical Interference Coatings 2016, OSA Technical Digest (online) (Optical Society of America, 2016)* **2016**, paper WB.9.
24. Woo, S.H.; Hwangbo, C.K. Influence of plasma ion-beam assistance on TiO₂ and MgF₂ thin films deposited by plasma ion-assisted deposition. *Surf. Coat. Technol.* **2007**, *201*, 8250-8257.
25. Liu, H.; Jensen, L.; Ma, P.; Ristau, D. Stress compensated anti-reflection coating for high power laser deposited with IBS SiO₂ and ALD Al₂O₃. *Appl. Surf. Sci.* **2019**, *476*, 521-527.
26. Jellison Jr., G.E.; Modine, F.A. Parameterization of the optical functions of amorphous materials in the interband region. *Appl. Phys. Lett.* **1996**, *69*, 371-373.
27. Fakhouri, H.N.; Hudaib, A.; Sleit, A. Multivector particle swarm optimization algorithm. *Soft Comput.* **2019**, 1-19.
28. Tikhonravov, A.; Trubetskov, M.; Amotchkina, T.; DeBell, G.; Pervak, V.; Sytchkova, A.K.; Grilli, M.L.; Ristau, D. Optical parameters of oxide films typically used in optical coating production. *Appl. Opt.* **2011**, *50*, C75-C85.

29. Amotchkina, T.; Trubetskov, M.; Tikhonov, A.; Angelov, I.B.; Pervak, V. Reliable optical characterization of e-beam evaporated TiO₂ films deposited at different substrate temperatures. *Appl. Opt.* **2014**, *53*, A8-A15.
30. Nezar, S.; Saoula, N.; Sali, S.; Faiz, M.; Mekki, M.; Laoufi, N.A.; Tabet, N. Properties of TiO₂ thin films deposited by rf reactive magnetron sputtering on biased substrates. *Appl. Sur. Sci.* **2017**, *395*, 172-129.
31. www.optilayer.com.
32. Kong, M.D.; Guo, C.; Li, B.C.; He, W.Y.; Wei, M. Fabrication of multi-wavelength visible and infrared filter for solar atmosphere tomographic imaging. *Chin. Opt. Lett.* **2017**, *15*, 123101.
33. Hilfiker, J.N.; Pribil, G.K.; Synowicki, R.; Martin, A.C.; Hale, J.S. Spectroscopic ellipsometry characterization of multilayer optical coatings. *Surf. Coat. Technol.* **2019**, *357*, 114-121.
34. Lv, Q.P.; Huang, M.L.; Deng, S.W.; Zhang, S.Q.; Li, G. Effects of oxygen flows on optical properties, micro-structure and residual stress of Ta₂O₅ films deposited by DIBS. *Optik* **2018**, *166*, 278-284.
35. Jena, S.; Tokas, R.B.; Thakur, S.; Udupa, D.V. Study of aging effects on optical properties and residual stress of HfO₂ thin film. *Optik* **2019**, *185*, 71-81.